Equilibrium position of a rigid sphere in a turbulent jet: A problem of elastic reconfiguration

T. Barois,[1] P. D. Huck,[2] M. Bourgoin,[2] and R. Volk[2]

[1]*Univ. Bordeaux, CNRS, LOMA, UMR 5798, F-33405 Talence, France*

[2]*Laboratoire de Physique, École Normale Supérieure de Lyon, Université de Lyon, CNRS, 46 Allée d'Italie, F-69364 Lyon, Cedex 07, France*

(Received 2 March 2017; revised manuscript received 2 June 2017; published 11 September 2017)

The position of floating spheres trapped within an immersed turbulent water jet is investigated. Using the self-similarity properties of the jet velocity profile, the equilibrium problem is formulated in a rescaled space where the sphere is static and deformable. This approach is found to be related to a problem of elastic reconfiguration where elasticity arises here from the geometry of the flow instead of an actual deformation of a body.

DOI: 10.1103/PhysRevE.96.033105

I. INTRODUCTION

Reconfiguration is a concept that was introduced in botany to describe plants in moving fluids [1]. Because a plant is deformable, its shape may change in a fluid flow. This results in a drag reduction compared to a reference configuration for an equivalent rigid body. The drag reduction is at the core of reconfiguration since the concept is usually associated to a survival strategy in high winds or fast currents [2–5].

The drag exerted on deformable structures has been studied in various contexts such as the study of plants in air [6] or water [7,8] flows and in simplified geometries corresponding to soft rods [9], rolled-up sheets [10], or flexible plates [11]. Contrary to a rigid body, the drag measured for those deformable structures is not proportional to the squared fluid velocity. Nevertheless, the drag D still verifies a simple scaling relation

$$D \sim V^{2+\mathcal{E}}, \tag{1}$$

where V is the fluid velocity and $\mathcal{E}$ a power exponent usually referred as the Vogel exponent.

The existence of a single scaling law (1) is a remarkable and robust result for many different situations. A first argument supporting this result is found by dimensional analysis based on the relevant physical parameters of the fluid-structure interaction problem [12]. A second complementary argument is found in the work of Alben *et al.* [9] in terms of self-similarity of the elastic structure profile. It should be mentioned that scaling laws with Vogel exponents (1) are also reported when the buoyant force [13], or equivalently the weight [14], is involved instead of elastic forces.

In this paper, a fluid-structure problem consisting of a rigid buoyant sphere placed in a self-similar flow is considered. While there is no deformation of the body, the framework of elastic reconfiguration is surprisingly adapted to describe the forces acting on the object. More precisely, it is shown that the fluid-structure interaction problem formulated in a specific rescaled frame is equivalent to a reconfiguration problem involving the isotropic deformation of an elastic body.

For all the practical situations where usual elastic reconfiguration is reported, deformable bodies are slender structures. For nonslender structures, reconfiguration is not likely to be observed as bulk deformations are not expected for a pressure drag ($\sim 10^3$ Pa for a wind of 30 m s^{-1}) that remains much smaller than the elastic modulus of usual materials ($\sim 10^9$ Pa) [5]. Beyond the exercise of interpreting a rigid-body problem as a problem of elasticity, the analogy that is proposed here permits the exploration of reconfiguration regimes for nonslender bodies such as spheres.

II. EXPERIMENTAL SETUP

The experimental setup studied here is depicted in Fig. 1. A turbulent monophasic jet is established in a water tank ($0.3 \times 0.3 \times 0.7$ m^3) by the injection of water through a circular nozzle with a diameter $d_N = 6.5$ mm. The flow rate Q in the experiments is between 10 and 50 mL s^{-1}, which corresponds to a velocity at the nozzle ranging from 0.3 to 1.5 m s^{-1}. The Reynolds numbers at the nozzle, Re_N, then vary between 2000 and 10 000, where $\mathrm{Re}_N = Q/d_N\nu$ with ν the kinematic viscosity of water. Floating polypropylene spheres (with density $\rho_s = 850$ kg m^{-3} and radius R ranging from 7 to 15 mm) are placed in the vicinity of the jet centerline and reach a stable equilibrium position where the buoyant force and the fluid forces are balanced. This configuration is similar to the levitation of a table-tennis ball over a hair dryer. The latter experiment is a classic teaching demonstration [15,16] exploiting the intriguing aspects of levitation [17].

The trapping stability of the sphere in the plane perpendicular to the jet axis has been discussed in terms of the Coandă effect [18]. If a curved surface is impacted by a jet, the outgoing jet is deflected, which imparts a net force on the curved body because of momentum conservation [19]. The Coandă effect and the associated forces have been investigated for spheres suspended by vertical [20] and tilted jets [21]. The trapping of spheres far from the nozzle is not observed. This is because the confining force in the horizontal plane decreases with the distance to the nozzle [20].

The question addressed here concerns the trapping distance between the sphere and the jet nozzle for a controlled injection flow rate. Despite its apparent simplicity, this problem is not trivial because it requires the computation of the force exerted by an inhomogeneous flow on a sphere. In the case of homogeneous flows, the computation of the drag involves an empirical coefficient known as the drag coefficient. For inhomogeneous flows, a similar empirical coefficient may exist [22] but it has no general formulation and depends on the geometry of the object as well as on the profile of the incoming flow.

The jet profile was determined by three-dimensional (3D) particle tracking velocimetry (PTV). Two cameras are used to record the tracks of submillimeter particles injected from the nozzle. The particles are matched in density with water in

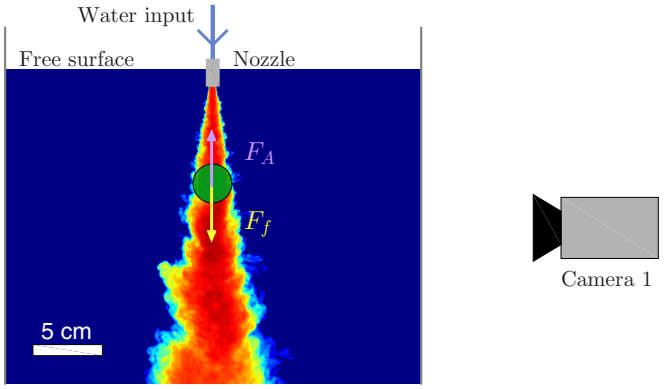

FIG. 1. Schematics of the trapped sphere experiment. Two cameras are positioned at 90° to observe the motion of the sphere in two perpendicular planes. The free jet profile is visualized from camera 2 (not represented) by the injection of dye at the nozzle. A solid circle is inserted to represent the typical trapping of a floating centimeter scale sphere submitted to buoyant forces and fluid forces with magnitudes F_A and F_f, respectively.

order to behave as tracers for the large-scale mean flow. The submillimeter particles are small enough to satisfy the uniform sampling condition [23] that occurs when the particles do not exceed 20 times the smallest scales of the turbulent flow. Here the size of the smallest scales is of the order of 0.1 mm. The 3D mean velocity map is obtained from the time averaging of the particle velocity onto a binning grid with submillimeter resolution. The radial profiles are extracted from the map for different distance z to the nozzle. Measurements of the mean profiles are performed for a flow rate of $Q = 27$ mL s^{-1} in the absence of the trapped sphere. Velocity profiles are displayed in Fig. 2 (left). The jet profile is self-similar when it is represented in a specific set of coordinates [24,25] as shown in Fig. 2 (right). The self-similar velocity profile is given by

$$v_z(r,z) = \frac{1}{z}\mathcal{F}\left(\frac{r}{z}\right), \tag{2}$$

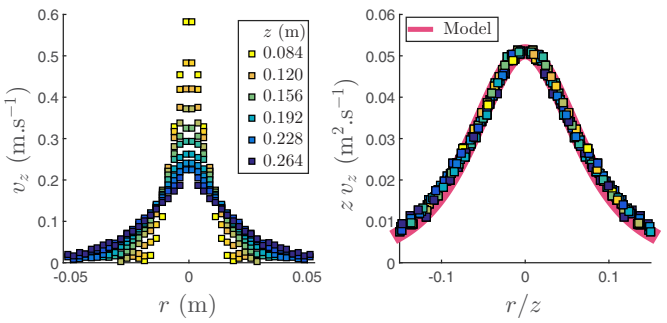

FIG. 2. Left: Axial velocity v_z of the jet as a function of the radial distance r. Eleven axial distances to the nozzle are considered for z starting from 84 mm going up to 264 mm with a linear spacing of 18 mm. The flow rate at the nozzle is $Q = 27$ mL s^{-1}. Right: Product zv_z (m^2 s^{-1}) as a function of the normalized radial coordinate r/z for the same data points. The solid line is a fitting function established after the profile $\mathcal{F}(r/z) \propto 1/(1+(r/\tan(\alpha)z)^2)^2$ [24] with $\alpha = 0.12$ rad.

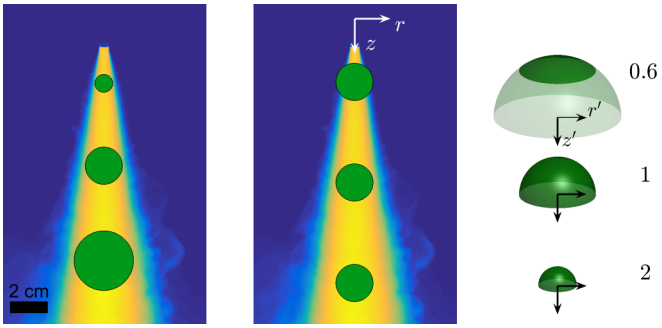

FIG. 3. Illustration of the self-similarity. Left: Three spheres with same drag for the same ratio z_e/R, where z_e is the equilibrium distance to the nozzle and R the sphere radius. Center: Three identical spheres at their equilibrium positions for three different flow rates. The cylindrical frame $\{r,z\}$ is represented at the origin of the jet. Right: Profiles in the rescaled frame $\{r' = r/z_e, z' = z/z_e\}$ of the spheres' surfaces impacted by the jet for the three corresponding positions of the central figure. The associated numbers indicate the radial portion of the sphere impacted by the jet in the scaled frame $\alpha z_e/R$, where α is the characteristic opening angle of the jet. This dimensionless number is interpreted as a Cauchy number [see Eq. (5)].

where r is the radial coordinate, z the vertical distance to the origin of the jet, and $\mathcal{F}$ the self-similar profile. The expression $\mathcal{F}(r/z) \propto 1/(1+(r/\tan(\alpha)z)^2)^2$ [24] is used for the fitting function in Fig. 2 (right). The parameter α relates to the opening half-angle of the jet with $\alpha = 0.12$ rad.

III. SELF-SIMILARITY

The stationary trapping of a sphere by a vertical jet occurs if the fluid forces and the buoyant forces are balanced (see Fig. 1). In this case, the magnitudes of these forces verify

$$F_A = F_f, \tag{3}$$

where F_f are the net fluid forces exerted on the sphere and F_A the buoyant forces given by the Archimedes principle $F_A = (4\pi/3)\Delta\rho R^3 g$, where R is the sphere radius, g the gravity field, and $\Delta\rho = \rho_w - \rho_s$ the apparent density with ρ_w the density of water and ρ_s the density of the sphere.

As mentioned before the expression F_f for the drag exerted on a spherical body in an inhomogeneous flow is a delicate problem. In this experiment, the sphere is only trapped close to the nozzle where the jet typical width does not exceed the sphere diameter. This means that the flow profile is strongly inhomogeneous over the sphere's surface and the presence of the sphere strongly modifies the flow profile. As a consequence, direct computation of the net fluid force acting on the sphere is challenging.

The strategy adopted here is to use geometric considerations related to the jet profile in order to reinterpret the vertical equilibrium position of a sphere. Because the jet profile is self-similar, the fluid forces acting on a sphere at a given position should be the same as the forces acting on a smaller sphere at a proportionally smaller distance to the origin of the jet. This geometrical property is sketched in Fig. 3 (left). If

self-similarity is verified, the fluid force may be written as

$$F_f = \mathcal{G}\left(\frac{R}{z_e}\right), \tag{4}$$

where z_e is the distance between the nozzle and the equilibrium position of the sphere. The function $\mathcal{G}$ depends on the jet profile (2) modified by the presence of the sphere.

The fluid force acting on a sphere in a jet [Eq. (4)] depends on the dimensionless radius R/z_e only. This means that a variation of the sphere position along the jet centerline z_e is equivalent to a decrease of the sphere radius R by the same factor (see Fig. 3).

The approach of this work is to consider the problem of the sphere trapped in the jet after the rescaling of the space coordinates $\{r,z\}$ by the factor z_e. In the dimensionless space $\{r',z'\}$, the sphere does not move as it lies at a distance unity ${z_e}' = 1$ from the nozzle. The sphere is effectively deformable with a radius $R' = R/z_e$. In the rescaled frame, the deformable sphere obeys a mechanical equilibrium with a stationary flow (Fig. 2, right).

IV. EFFECTIVE RECONFIGURATION

The study of drag reduction in reconfiguration problems uses two dimensionless parameters: the Cauchy number C_Y and the reconfiguration number $\mathcal{R}$.

The Cauchy number quantifies the deformation induced by the fluid flow by comparing the fluid dynamic pressure σ_f and the elastic stress σ_E for a typical deformation. For usual reconfiguration problems, i.e., with an actual elastic deformable body, the typical elastic stress is the elastic Young modulus E, and the Cauchy number is given by $C_Y = \sigma_f/E$. For the problem addressed here, there is *a priori* no expression for an elastic modulus. However, a Cauchy number can be proposed by considering a generic elastic relation $\sigma_f = E\epsilon$ that the deformable sphere would verify in the rescaled frame, where σ_f is the external stress due to the fluid and ϵ is the resulting deformation ratio. In this case, the Cauchy number is simply given by $C_Y = \epsilon$. In the rescaled frame, the deformation of the sphere corresponds to an isotropic deformation for which the strain in the linear regime is $\epsilon \sim \delta R/R$. As the variation of R and z_e is equivalent, the strain parameter may scale as $\epsilon \sim z_e/R$. In the following, the Cauchy number is defined by

$$C_Y = \alpha\frac{z_e}{R}, \tag{5}$$

where the opening angle of the jet, α, has been introduced.

The reconfiguration number $\mathcal{R}$ quantifies the efficiency of the drag reduction by comparing the drag exerted on the deformable body and the drag that would be exerted on the equivalent rigid body. As mentioned before, the drag exerted on the sphere equals the buoyancy. The drag on the equivalent rigid body corresponds to the drag in the limit $\epsilon = 0$. In this limit, the sphere is asymptotically close to the jet nozzle and impacted on its top surface which is perpendicular to the flow. Consequently one can write the reconfiguration number as

$$\mathcal{R} = \frac{(4\pi/3)\Delta\rho R^3 g}{(1/2)c_P\rho_w(Q^2/S_N)}, \tag{6}$$

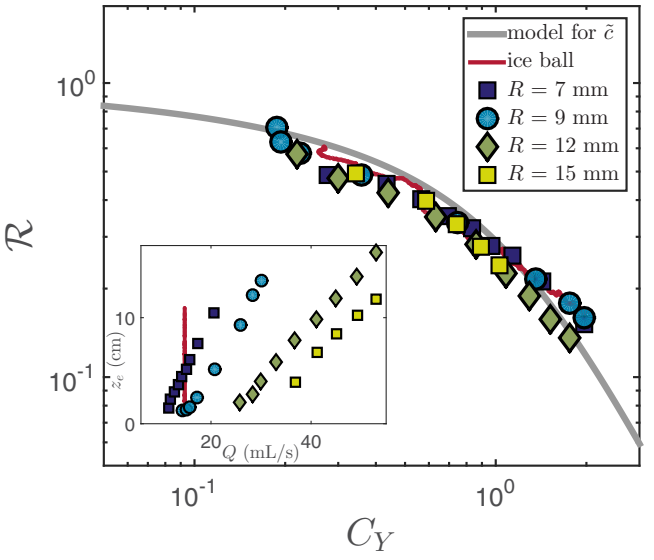

FIG. 4. Reconfiguration number [Eq. (6)] as a function of the Cauchy number [Eq. (5)] for polypropylene spheres and a melting ice ball. The solid line corresponds to the equilibrium problem (3) with an empirical expression for the drag coefficient, $\tilde{c}(r/R) = 1 - (r/R)^\eta$, with $\eta = 0.5$. The inset plot shows the equilibrium distance to the nozzle,z_e, as a function of the flow rate Q for the same data points.

where $c_P = 2.1$ is the drag coefficient of a plate for the jet profile and $S_N = (\pi/4){d_N}^2$ the cross-sectional area of the nozzle.

The equilibrium positions of spheres for varying flow rates of the jet have been measured for a set of four floating spheres and a melting spherical ice ball. The ice ball was obtained by crystallization of dyed water in a specific mold previously designed [26]. The relative density is 0.85 for the polypropylene spheres and 0.92 for the ice ball. The average positions of the spheres are obtained from acquisitions of 45 s, corresponding to an order of 10^2 oscillations of the sphere in the confining potential with a typical amplitude $\sim R$. The resulting data are plotted in Fig. 4 using the dimensionless numbers C_Y and $\mathcal{R}$ defined in Eqs. (5) and (6). For comparison, the equilibrium distance with respect to the flow rate has been also represented in usual coordinates in the inset plot in the same figure.

The experimental data collapse on a master curve when represented with the dimensionless numbers C_Y and $\mathcal{R}$. This master curve shows a quantitative agreement with reconfiguration of actual deformable bodies in a flow (see [5] for example).

The limit $C_Y \ll 1$ relates to a low drag limit where the deformable body in the rescaled space is weakly deformed. This implies that the drag is that of an equivalent rigid body ($\mathcal{R} \sim 1$). In physical space, this limit corresponds to a sphere impacted by the jet at its very center where the sphere is locally a surface perpendicular to the flow. According to its definition, the reconfiguration number is expected to approach unity in the low drag limit where deformation is asymptotically small. This is the case here, notably because the parameter c_P has been introduced to account for the drag of the sphere when it is close to the jet nozzle.

For $C_Y \sim 1$, the body is moderately deformed. The reconfiguration and drag reduction are dominated by the streamlining of the body rather than the area reduction [11]. In physical space, this regime corresponds to the jet impacting the sphere on its typical size. This justifies the introduction of the opening angle $\alpha = 0.12$ rad in the expression of the Cauchy number since this transition is expected for $C_Y \sim 1$.

For higher Cauchy numbers, the whole sphere is impacted by the jet and the drag reduction may be attributed to the area reduction in the rescaled frame. In physical space, the sphere is far from the nozzle, $z_e > R/\alpha$, and in a spatially homogeneous flow corresponding to the axial velocity on the jet centerline [27]. In this regime of uniform flow, the drag is $1/2 c_s \rho_w \pi R^2 {v_e}^2$, where c_s is the drag coefficient for a sphere and v_e the equilibrium velocity needed to balance buoyancy. The asymptotic regime $C_Y \gg 1$ is not observed for trapped spheres since the confinement is not possible without velocity gradients. The stationary trapping is experimentally lost around $C_Y \sim 2$. If stability was possible for $C_Y \gg 1$, one should expect a scaling regime for the reconfiguration number where $\mathcal{R} \sim {C_Y}^{-2}$ (or a Vogel exponent $\mathcal{E} = -2$) after the definition of $\mathcal{R}$ and the expression for the equilibrium velocity on the centerline, $v_e = v(r = 0, z_e) \propto (1/z_e) Q/S_N$. This regime could be explored by a force measurement while maintaining the sphere in the jet.

The relation between $\mathcal{R}$ and C_Y has also been explored for a given flow rate $Q = 18$ mL s^{-1} with a melting ice ball as plotted in Fig. 4. Contrary to an attached body [28], the melting is isotropic because the ice ball is free to rotate when it is suspended in the jet. This experiment allows for a continuous variation of $\mathcal{R}$ and C_Y as the ball progressively melts and reduces in size. As for the rigid spheres, the equilibrium is lost when C_Y approaches 2.

The collapse of the data in Fig. 4 implies that, in the rescaled frame, the sphere behaves as a deformable body with a stress-to-strain relation similar to Hooke's law. The analogy with reconfiguration allows for the introduction of an effective elastic coefficient for the sphere. For an elastic body, the Cauchy number is given by $C_Y = \rho U^2/E$, where ρ is the density of the fluid, U the flow velocity, and E the elastic modulus. With this relation considered for $C_Y = 1$, one obtains an effective elastic modulus $\tilde{E} = \rho_w (Q/S_N)^2$.

In Sec. III, the self-similarity of the fluid force [Eq. (3)] has been assumed as it is suggested by the self-similar properties of the jet flow. The net force [Eq. (4)] can be explicitly obtained from the jet profile [Eq. (2)] by integrating a simplified model for local drag over the sphere cross section,

$$dF_f(r,z) = (1/2)\rho_w \tilde{c}(r/R) v_z(r,z)^2 \, dS, \tag{7}$$

where $\tilde{c}$ is a dimensionless local drag coefficient. This approach is usual for slender structures where the local drag description is valid. Here, the flow around a sphere is highly nonlocal which means that inconsistencies are expected. The empirical expression $\tilde{c}(r/R) = c_P(1 - (r/R)^\eta)$ is used in a local drag approach [Eq. (7)], where $c_P = 2.1$ is the drag coefficient for a perpendicular plate and the exponent $\eta = 0.5$ is the only free parameter used to obtain a satisfactory fit of the rescaled data in Fig. 4. However, the local drag approach and the expression of $\tilde{c}$ are limited to this experiment as they are not valid, for instance, for a sphere in a uniform flow: $v_z(r, z_e) = v_0$.

V. CONCLUSION AND PERSPECTIVES

In this paper, we have proposed an original approach to account for the equilibrium position of a sphere trapped by a turbulent jet. It was shown that the existence of self-similar forces establishes a connection with a problem of elasticity based on a geometric interpretation of self-similarity. In this interpretation, the space may be rescaled which means that the sphere is static but deformable.

A relation similar to linear elasticity was proposed to account for the mechanical equilibrium of the sphere in the rescaled coordinates. The representation of reconfiguration based on the dimensionless numbers $\mathcal{R}$ and C_Y shows remarkable similarities with classical reconfiguration studies involving the actual deformation of a truly elastic body. With this analogy, it is possible to define an effective elastic modulus for the deformable sphere in the rescaled frame.

The asymptotic regime of high deformation, $C_Y \gg 1$, or equivalently $z_e \gg R/\alpha$, is not accessible for a trapped sphere. This is because the confining associated with the velocity gradients of the jet profile is too weak to overcome the forces induced by the velocity fluctuations of the fluid. However, reconfiguration in this regime is predictable because the velocity is homogeneous on the scale of the sphere with a simple scaling on the centerline, $v(r = 0, z) \propto z^{-1}$. The asymptotic regime $C_Y \gg 1$, where $\mathcal{R} \, \alpha \, {C_Y}^{-2}$ would be observed by maintaining the sphere in the jet centerline where the vertical forces vanish.

Future work following this contribution may consider a usual reconfiguration experiment with spheres truly capable of deformation. The center of the soft sphere should be maintained in a fixed position in the similar jet flow. A technical difficulty would be to manufacture an elastic spherical body for which the deformations are purely isotropic. A promising approach would be to use a class of soft mechanical metamaterials [29–31] close to the limit of dilational elasticity [32]. The dilational regime corresponds to the pure extensional deformations, which means with a Poisson ratio that is equal to -1. In this limit, the only deformation modes allowed are the ones that change the size of the object but not its shape. In these conditions, some unconventional regime of reconfiguration could be observed for a nonslender metamaterial body, such as regimes of drag independent of the flow velocity, that was only reported in a previous work [14] for slender structures.

[1] S. Vogel, Amer. Zool. **24**, 37 (1984).
[2] A. R. Ennos, J. Exp. Bio. **202**, 3281 (1999).
[3] K. J. Niklas, New Phytol. **143**, 19 (1999).
[4] L. H. Harder, O. Speck, C. L. Hurd, and T. Speck, J. Plant Growth Regul. **23**, 98 (2004).
[5] E. de Langre, Annu. Rev. Fluid Mech. **40**, 141 (2008).

[6] S. Vogel, J. Exp. Bot. **40**, 941 (1989).
[7] K. Sand-Jensen, Freshwater Biol. **48**, 271 (2003).
[8] H. M. Nepf, J. Hydraul. Res. **50**, 262 (2012).
[9] S. Alben, M. Shelley, and J. Zhang, Nature (London) **420**, 479 (2002).
[10] L. Schouveiler and A. Boudaoud, J. Fluid Mech. **563**, 71 (2006).
[11] F. Gosselin, E. de Langre, and B. A. Machado-Almeida, J. Fluid Mech. **650**, 319 (2010).
[12] E. de Langre, A. Gutierrez, and J. Cossé, C. R. Mec. **340**, 35 (2011).
[13] M. Luhar and H. M. Nepf, Limnol. Oceanogr. **56**, 2003 (2011).
[14] T. Barois and E. de Langre, J. Fluid Mech. **735** (2013).
[15] J. Güémez, C. Fiolhais, and M. Fiolhais, Phys. Educ. **44**, 53 (2009).
[16] T. López-Arias, Eur. J. Phys. **33**, 253 (2012).
[17] E. H. Brandt, Science **243**, 349 (1989).
[18] R. Wille and A. Fernholz, J. Fluid Mech. **23**, 801 (1965).
[19] T. A. Vil'gel'mi, J. Appl. Mech. Tech. Phys. **10**, 754 (1969).
[20] T. López-Arias, L. M. Gratton, G. Zendri, and S. Oss, Phys. Educ. **46**, 146 (2011).
[21] J. Feng and D. D. Joseph, J. Fluid Mech. **315**, 367 (1996).
[22] S. Davoust and L. Jacquin, in *Sixth International Symposium on Turbulence and Shear Flow Phenomena* (Begell House, Danbury, CT, 2009), pp. 1237–1242.
[23] N. Machicoane, R. Zimmermann, L. Fiabane, M. Bourgoin, J.-F. Pinton, and R. Volk, New J. Phys. **16**, 013053 (2014).
[24] S. B. Pope, *Turbulent Flows* (Cambridge University Press, Cambridge, UK, 2000).
[25] I. Wygnanski and H. Fiedler, J. Fluid Mech. **38**, 577 (1969).
[26] N. Machicoane, J. Bonaventure, and R. Volk, Phys. Fluids **25**, 125101 (2013).
[27] K. T. McDonald, Am. J. Phys. **68**, 388 (2000).
[28] L. Ristroph, M. N. J. Moore, S. Childress, M. J. Shelley, and J. Zhang, Proc. Natl. Acad. Sci. USA **109**, 19606 (2012).
[29] J. Shim, C. Perdigou, E. R. Chen, K. Bertoldi, and P. M. Reis, Proc. Natl. Acad. Sci. USA **109**, 5978 (2012).
[30] S. Babaee, J. Shim, J. C. Weaver, E. R. Chen, N. Patel, and K. Bertoldi, Adv. Mater. **25**, 5044 (2013).
[31] C. Coulais, Int. J. Solids Struct. **97**, 226 (2016).
[32] T. Bückmann, R. Schittny, M. Thiel, M. Kadic, G. W. Milton, and M. Wegener, New J. Phys. **16**, 033032 (2014).